
Figures and figure supplements

Evolutionary adaptation of an HP1-protein chromodomain integrates chromatin and DNA sequence signals

Lisa Baumgartner *et al.*

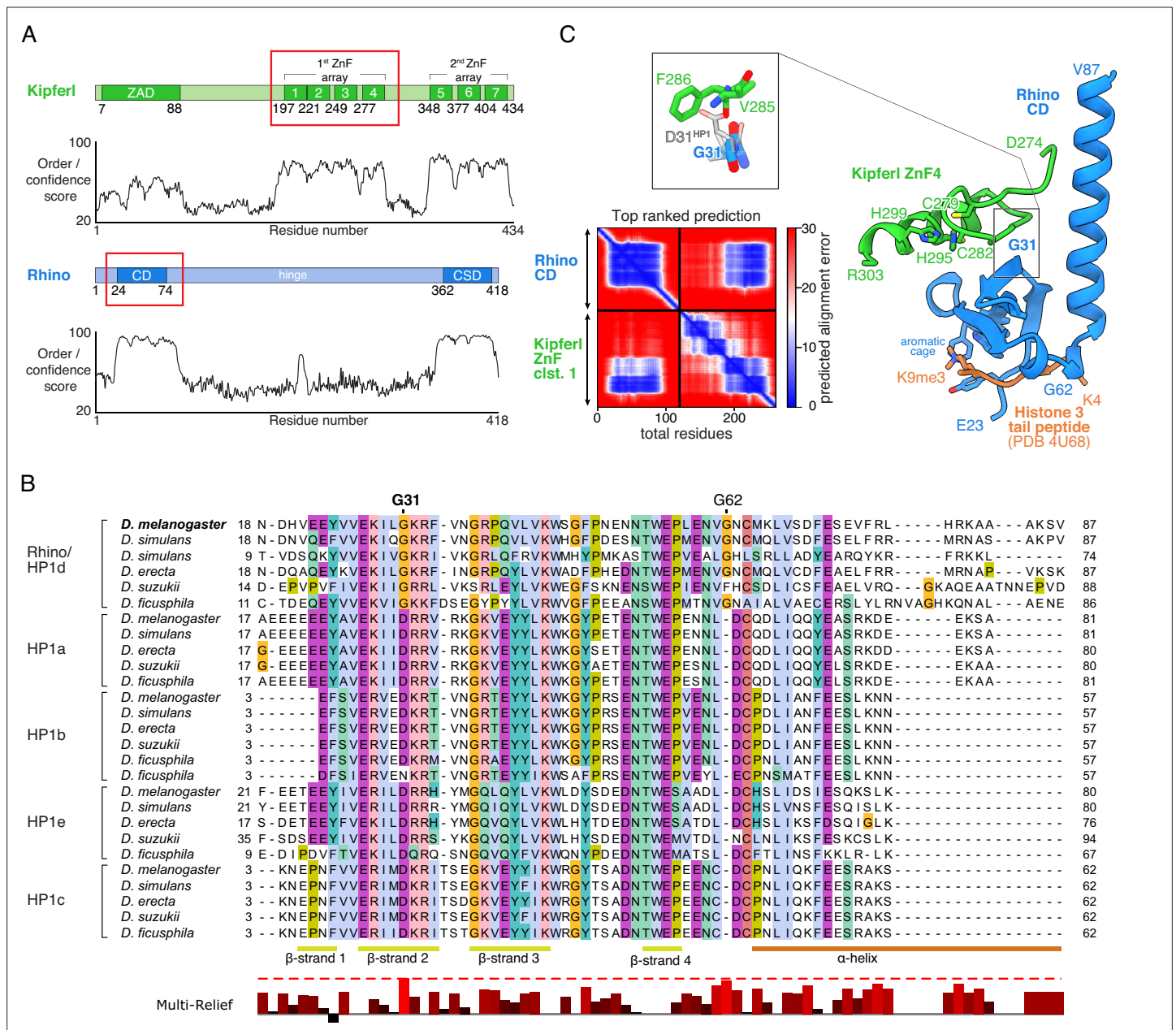


Figure 1. Structure prediction and phylogenetic analyses point to a Rhino-specific residue involved in binding Kipferl. **(A)** Domain organization of Kipferl and Rhino, with the AlphaFold2 Multimer predicted local distance difference test (pLDDT) score plotted as a measure of order or disorder alongside. Red boxes indicate the smallest interacting fragments identified by yeast two-hybrid experiments by [Baumgartner et al., 2022](#). ZAD, zinc finger-associated domain; ZnF, zinc finger; CD, chromodomain; CSD, chromo shadow domain. **(B)** Multiple sequence alignment of heterochromatin protein 1 (HP1) family proteins in five selected species harboring an unequivocally identified Kipferl homolog (see [Figure 1—figure supplement 2](#)). Rhino-specific amino acid residues are indicated. Protein accessions and identifiers are documented in [Supplementary file 1](#). Multi-Relief representation indicates residues that differ significantly in Rhino homologs versus other HP1 variant proteins. Note that two Rhino paralogs are identified in *D. simulans* (see [Supplementary file 1](#) for accessions). **(C)** Predicted aligned error (PAE) plot for the top ranked AlphaFold2 Multimer prediction of the Rhino chromodomain with the Kipferl ZnF cluster 1 (left) and structure of the complex in cartoon representation (Rhino in blue; Kipferl in green), together with the H3K9me3 peptide (orange) as observed in a Rhino-H3K9me3 crystal structure (PDB ID 4U68). Key residues of Rhino's aromatic cage and H3K9me3, as well as of Kipferl's C₂H₂ ZnF4 are shown in sticks representation. Only the interacting ZnF4 is shown. Depicted in the inset are Rhino G31 and HP1 D31, with HP1 (PDB ID 6MHA) superimposed on Rhino chromodomain residues 26–57 (root mean square deviation = 0.55 Å), together with Kipferl V285 and F286, illustrating that D31 would lead to steric clashes with Kipferl.

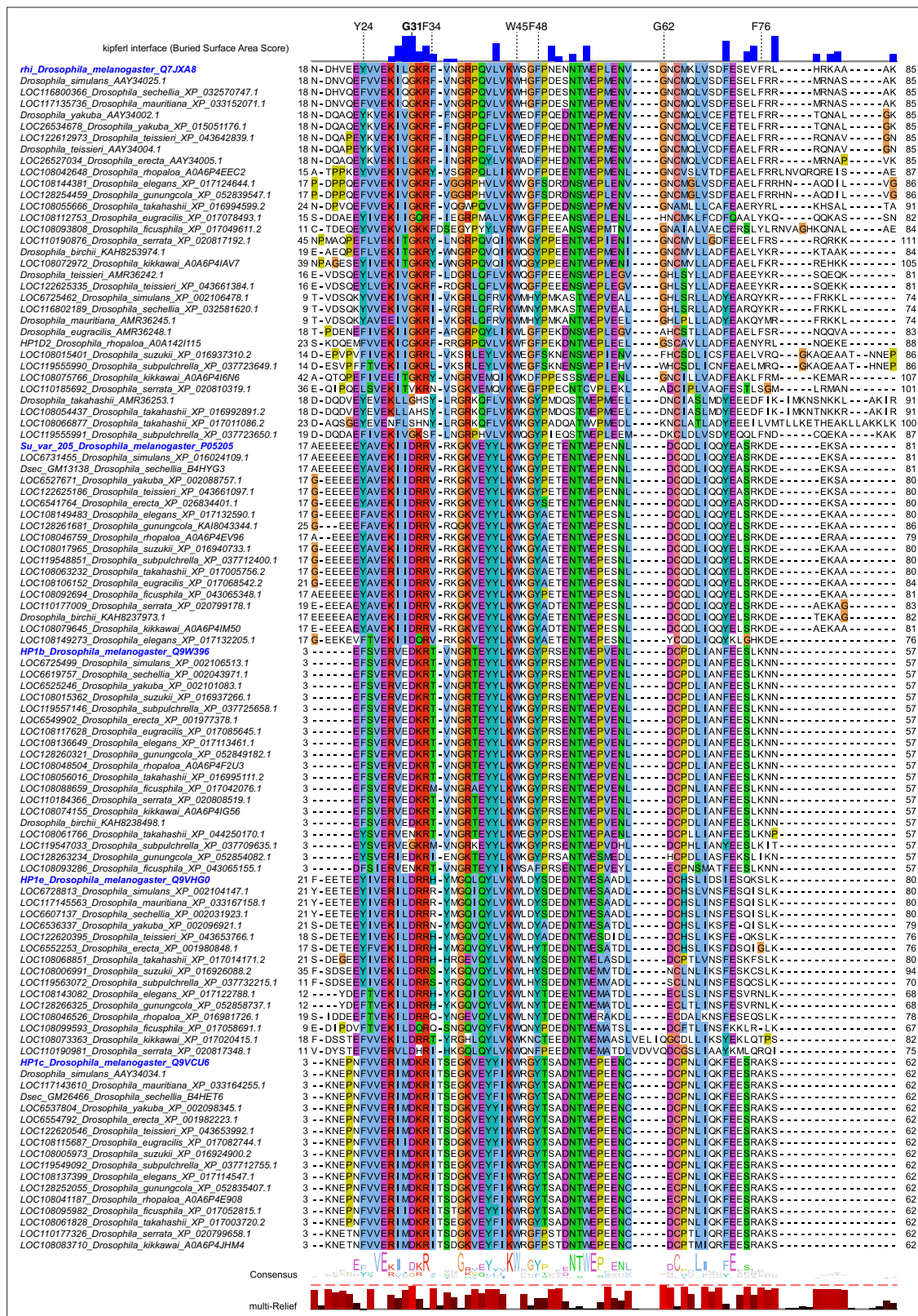


Figure 1—figure supplement 1. Multiple sequence alignment of heterochromatin protein 1 (HP1) family proteins across *Drosophila* species. Further details on protein accessions and identifiers are documented in **Supplementary file 1**. Buried surface area score (Krissinel and Henrick, 2007) in blue indicates residues involved in contacts with Kipferl based on the models predicted by AlphaFold2 Multimer. Multi-Relief representation indicates residues that differ significantly from Rhino homologs versus other HP1 variant proteins.

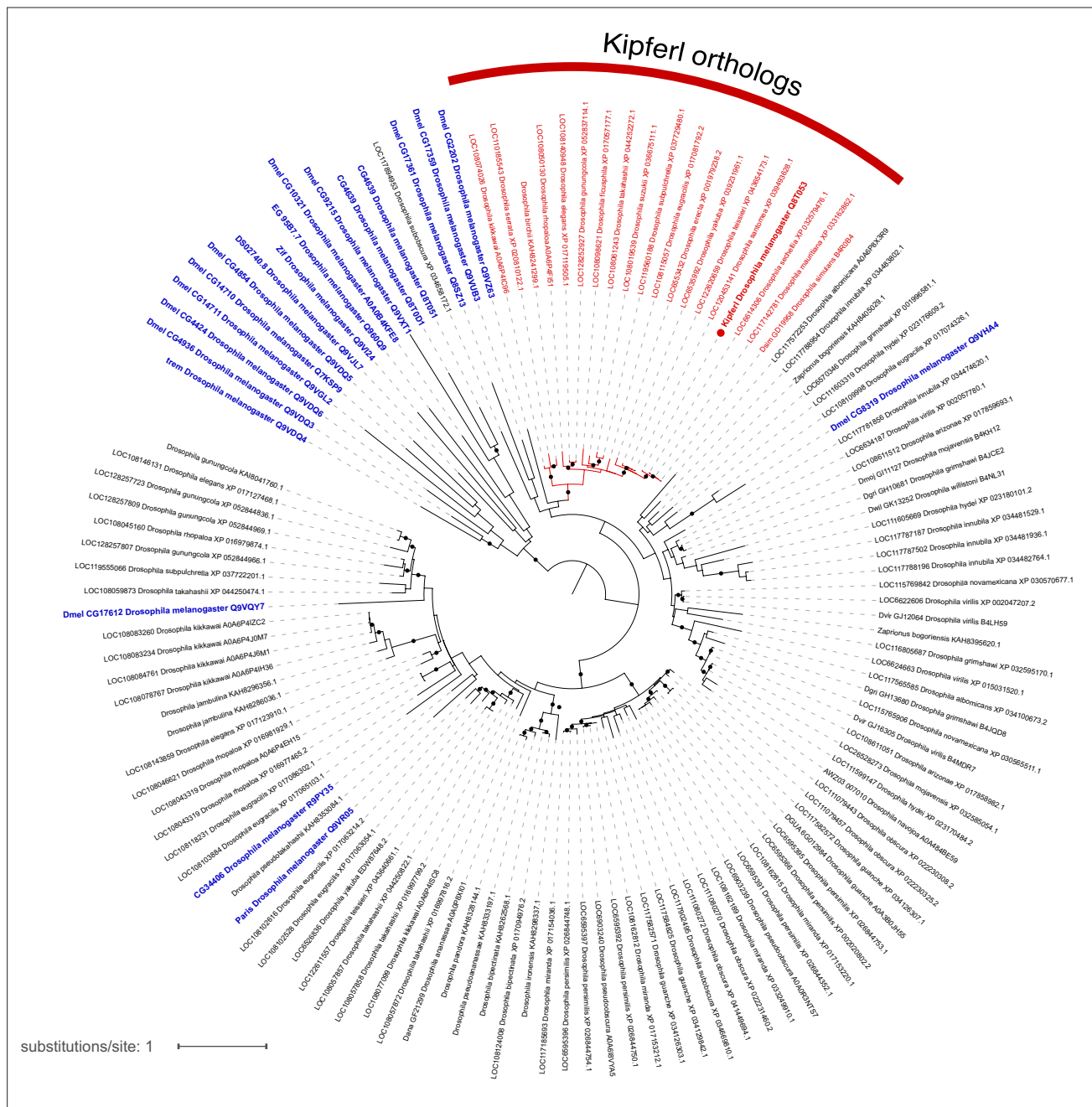


Figure 1—figure supplement 2. Phylogenetic tree illustrating the evolutionary relationship of zinc finger-associated domain (ZAD)-containing zinc finger proteins based on ZAD protein sequence. Blue labels indicate *Drosophila melanogaster* proteins, red labels mark Kipferl orthologs in different species. Branches that are supported by an ultrafast bootstrap (UFBoot) value $\geq 95\%$ are indicated by a black dot. Branch lengths represent the inferred number of amino acid substitutions per site, and branch labels are composed of gene name (if available), genus, species, and accession number.

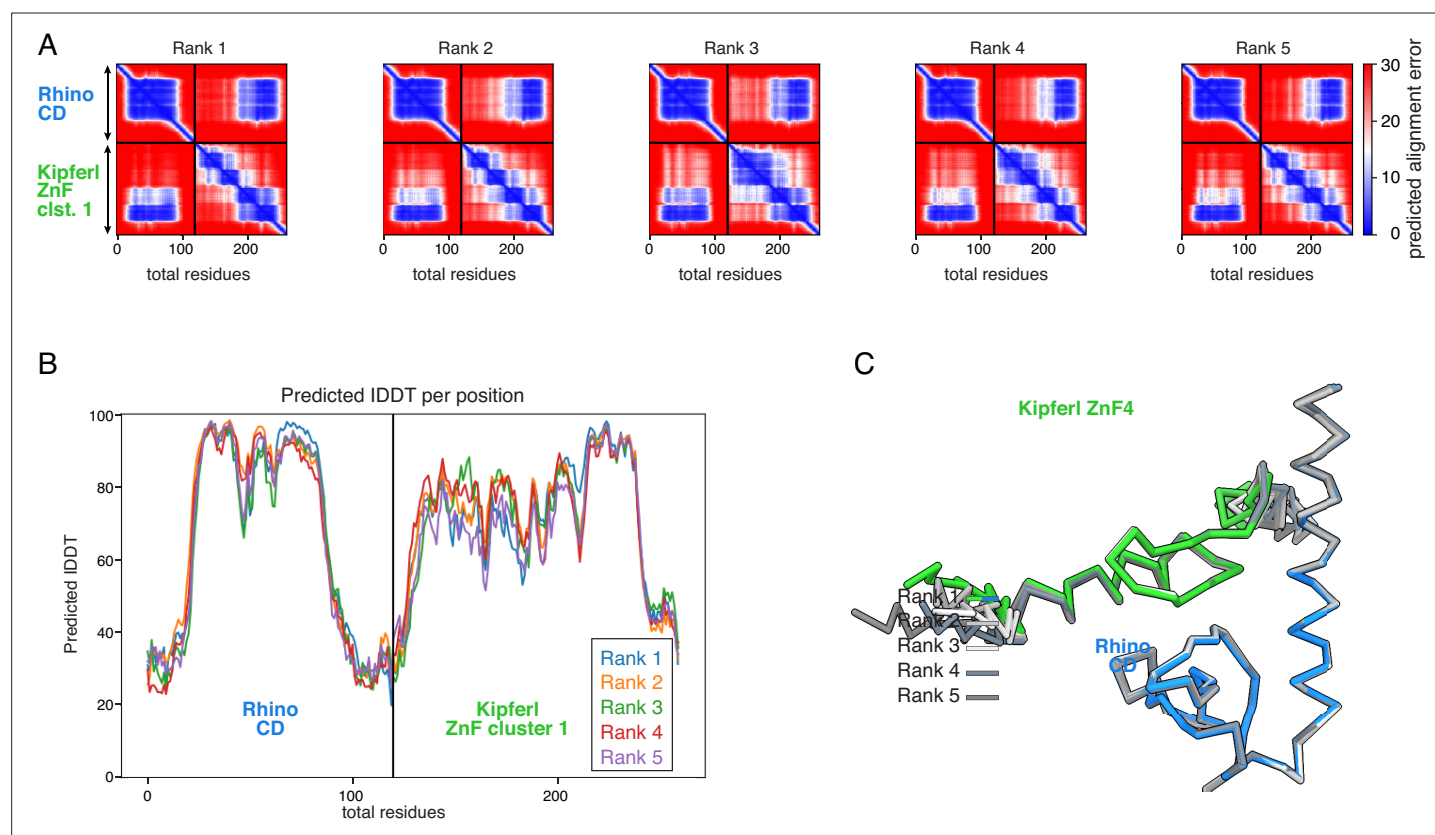


Figure 1—figure supplement 3. Diagnostic plots for ranks 1–5 for the AlphaFold2 Multimer prediction of the Rhino chromodomain with the Kipferl ZnF cluster 1. (A) PAE plots. (B) pLDDT plot. (C) Superposition on the Rhino chromodomain of the models for ranks 1–5, as C α trace.

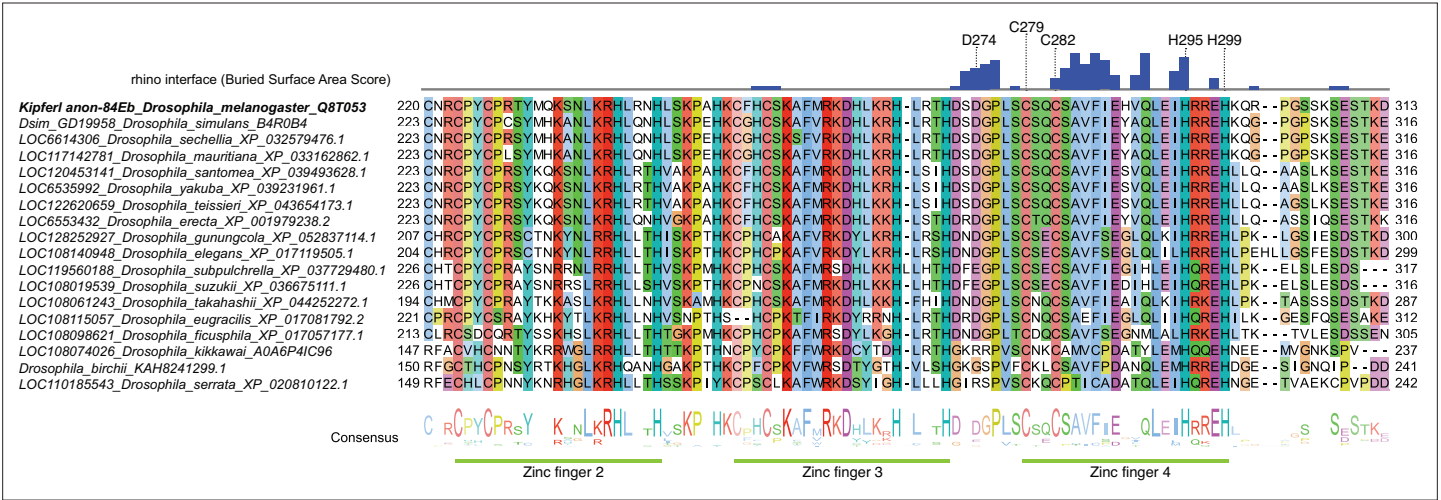


Figure 1—figure supplement 4. Multiple sequence alignment of Kipferl proteins across *Drosophila* species. Buried surface area score in blue (**Krissinel and Henrick, 2007**) indicates residues involved in contacts with Rhino based on the models predicted by AlphaFold2 Multimer. Labeled residues correspond to those highlighted in **Figure 1C**.

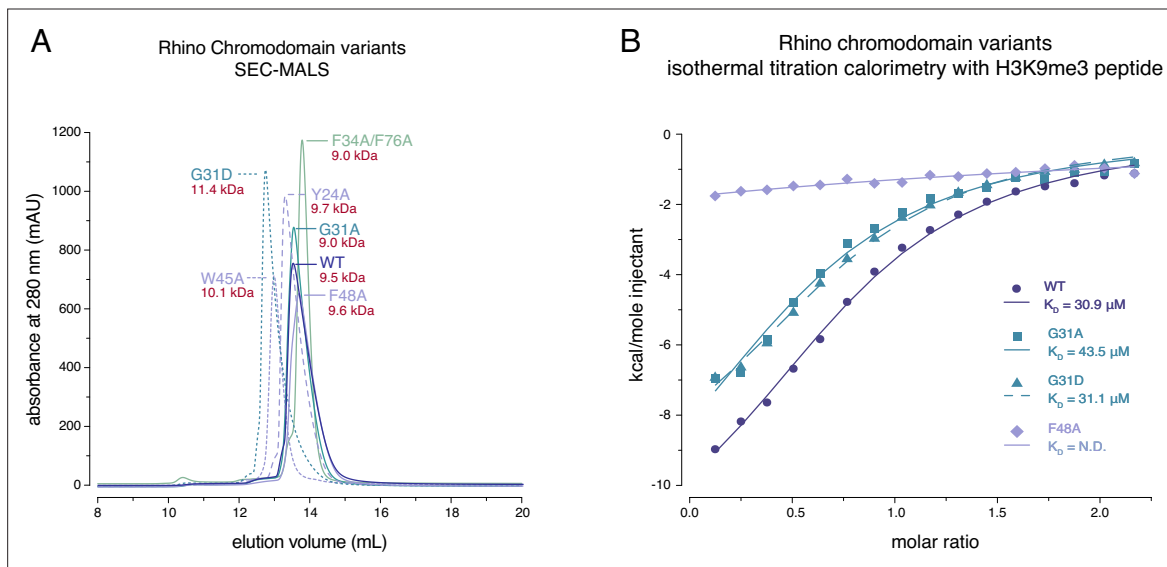


Figure 2. Rhino G31 point mutations do not affect Rhino's ability to bind H3K9me3. **(A)** Line graph summarizing size-exclusion chromatography with inline multiangle light scattering (SEC-MALS) results for the examined Rhino chromodomain constructs. The in solution molecular weight is indicated for each construct. **(B)** Isothermal titration calorimetry results showing the binding of indicated Rhino chromodomain constructs to the H3K9me3-modified histone tail peptide.

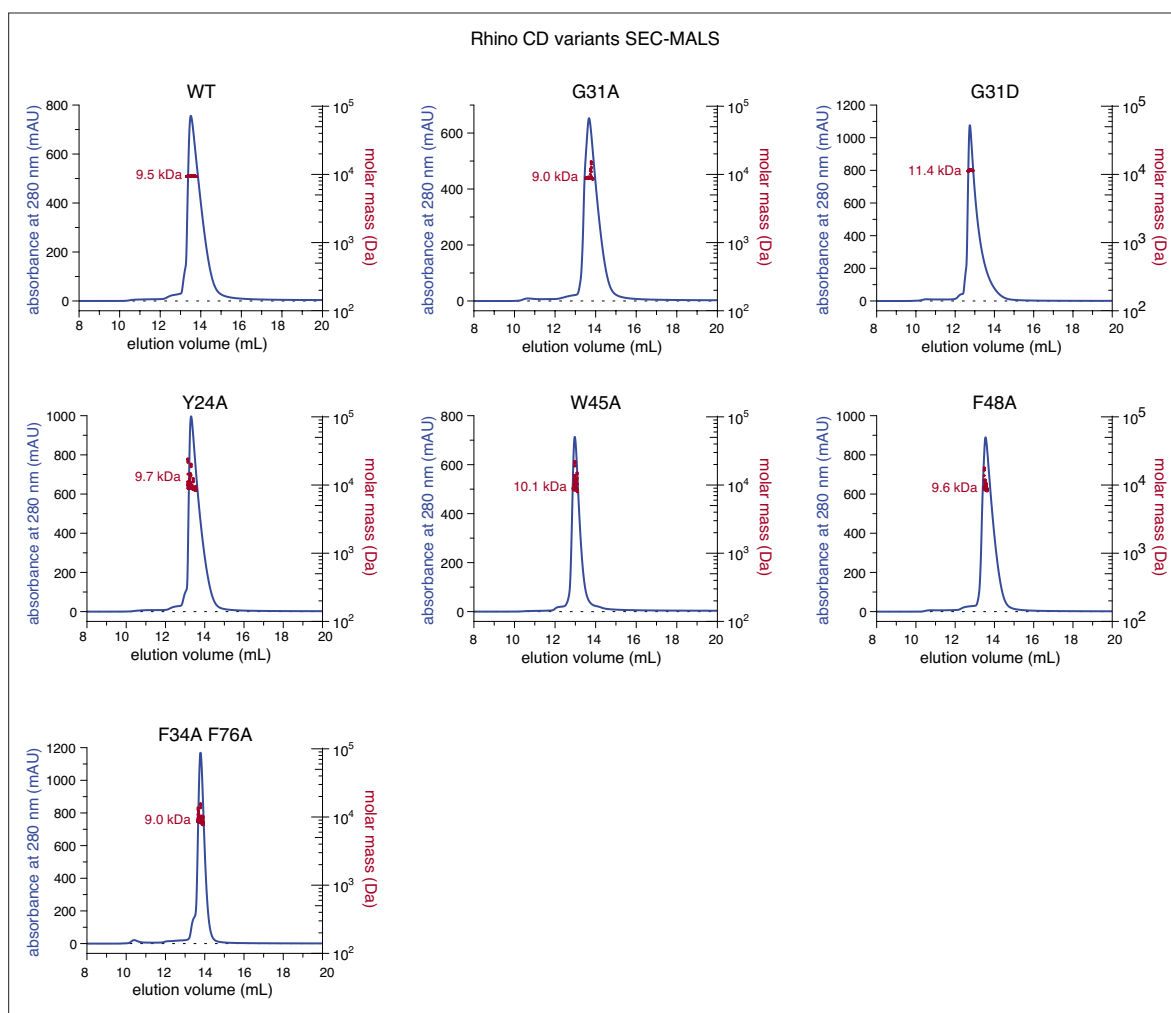


Figure 2—figure supplement 1. Individual line graphs depicting size-exclusion chromatography with inline multiangle light scattering (SEC-MALS) results for the examined Rhino chromodomain constructs with in solution molecular weight measurements depicted in red.

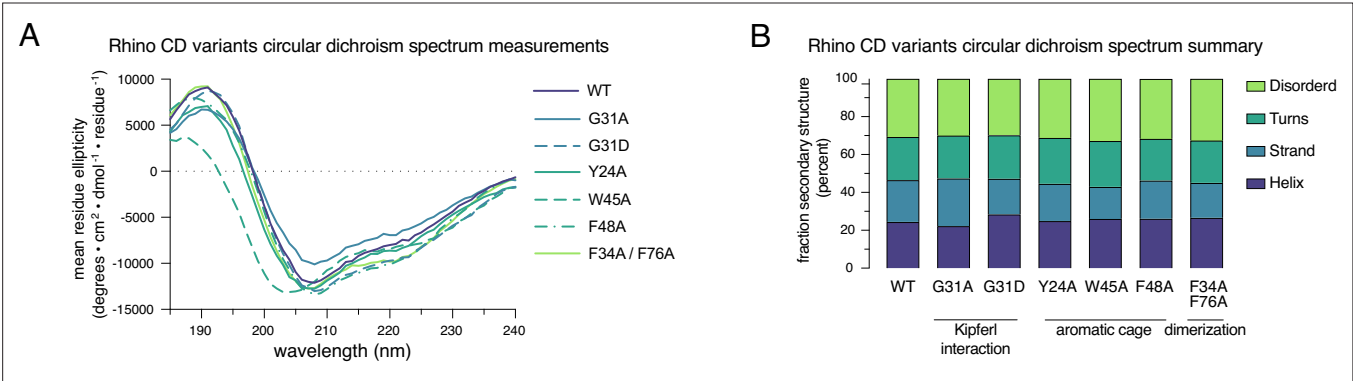


Figure 2—figure supplement 2. Purified Rhino point mutant chromo domains display normal protein folding. **(A)** Raw circular dichroism spectrum plots comparing the ellipticity versus wavelength for tested Rhino chromodomain constructs. **(B)** Bar graph summarizing circular dichroism spectrum measurements for the tested Rhino chromodomain constructs.

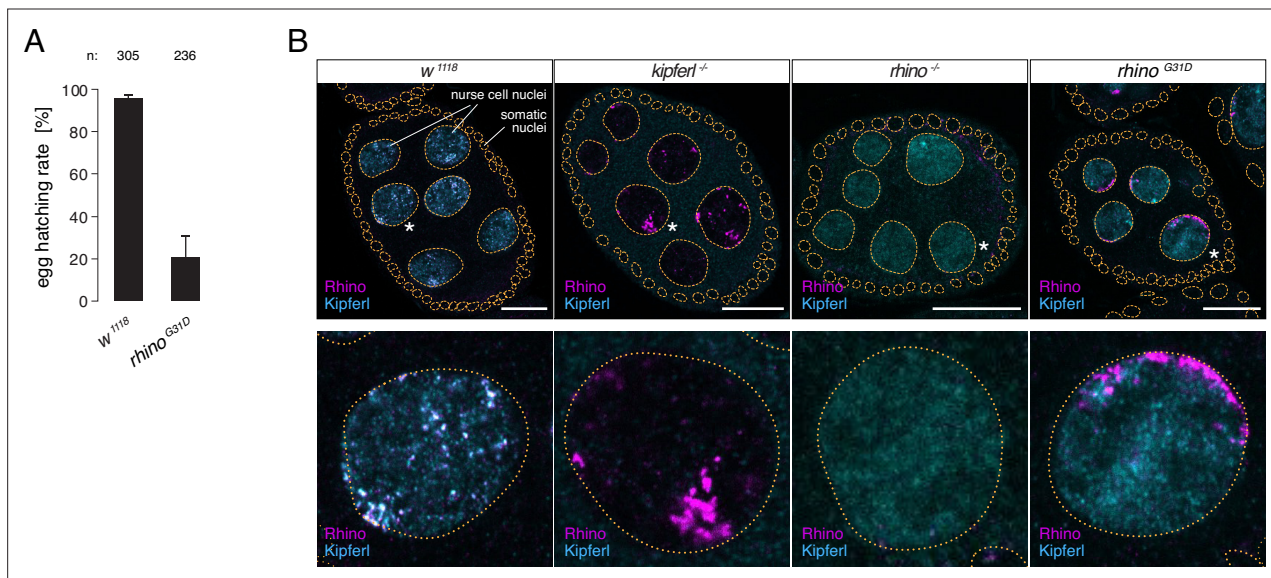


Figure 3. The *rhino^{G31D}* point mutation recapitulates the phenotypes for Rhino and Kipferl in each other's null-mutant background. **(A)** Bar graph depicting female fertility as egg hatching rate in percent of laid eggs for indicated genotypes. Error bars indicate standard deviation of three technical replicates. The total number of eggs assessed across all replicates is given as n. **(B)** Confocal images showing immunofluorescence signal for Kipferl and Rhino in egg chambers of indicated genotypes. Zoomed images display one representative nurse cell nucleus (labeled by white asterisk in panel A) per genotype (scale bar: 20 μ m).

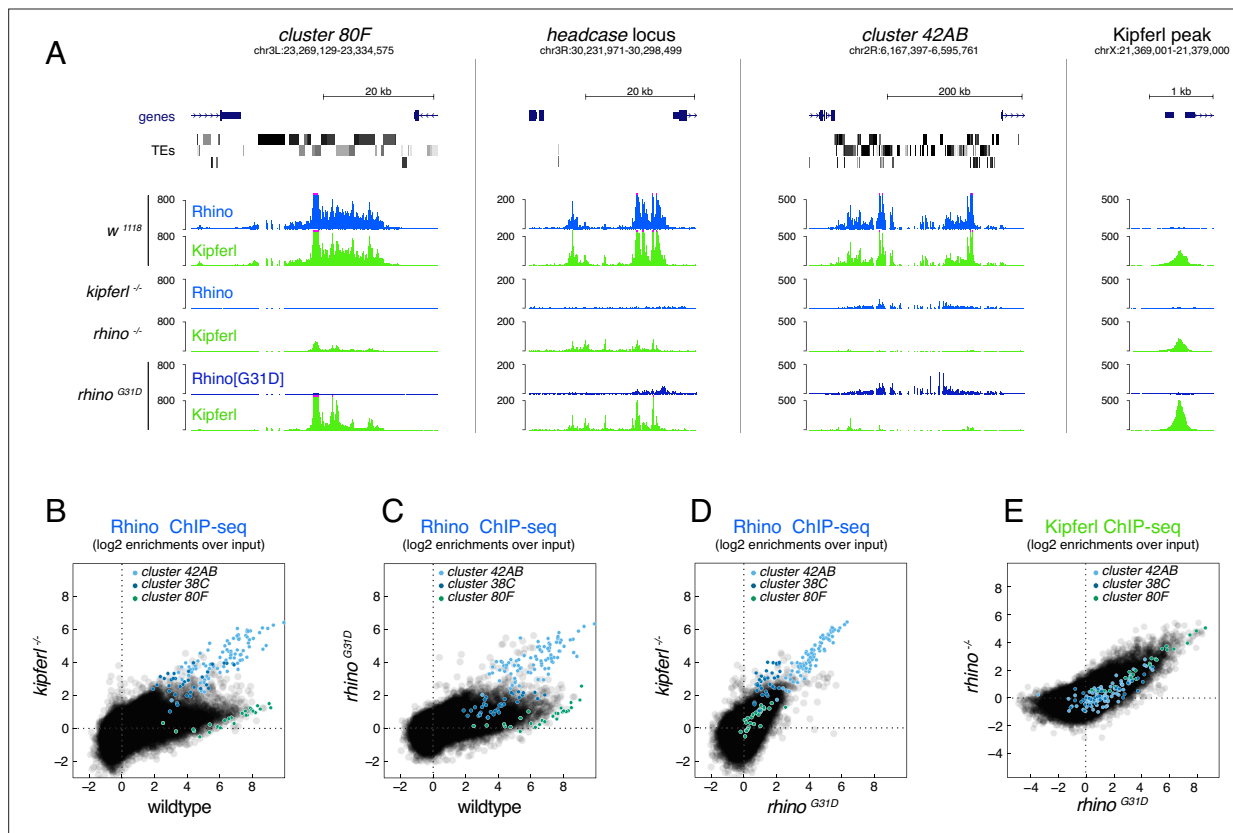


Figure 4. The Rhino^{G31D} point mutation uncouples Rhino and Kipferl on chromatin. **(A)** UCSC genome browser screenshots depicting the ChIP-seq signal for Rhino and Kipferl at diverse Rhino domains in ovaries of the indicated genotypes (signal shown as coverage per million sequenced reads for one representative replicate). Scatter plot of genomic 1-kb tiles contrasting average log2-fold ChIP-seq enrichment for Rhino (**B–D**) or Kipferl (**E**) in ovaries of the indicated genotypes (values displayed represent the average of two to three replicate experiments).

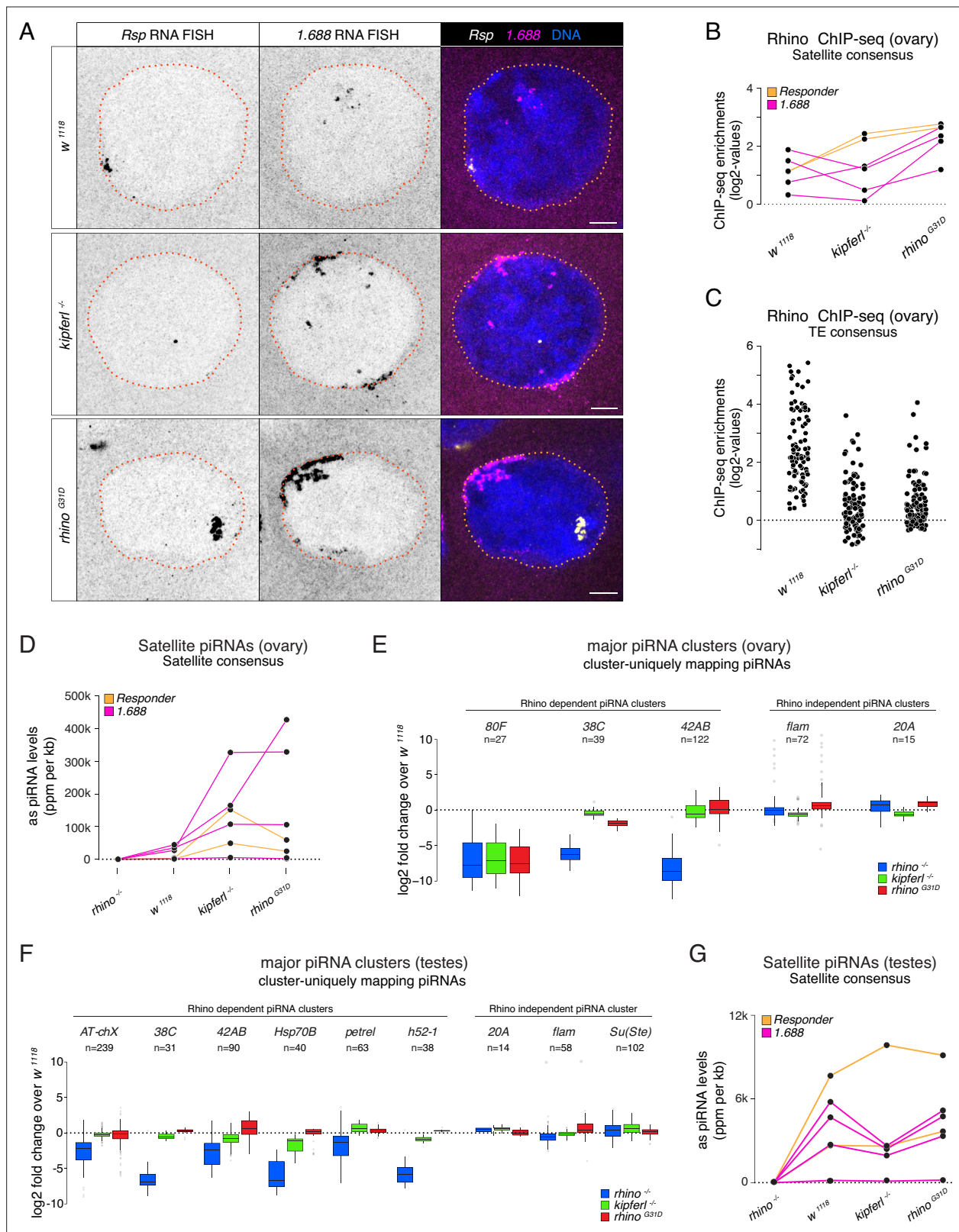


Figure 5. Kipferl-independent functions of Rhino are not affected by the G31D mutation. **(A)** Confocal images showing *Rsp* and 1.688g/cm³ Satellite RNA fluorescent in situ hybridization (FISH) signal in nurse cells of indicated genotypes (scale bar: 5 μ m). Jitter plots depicting the log₂-fold enrichments for Rhino ChIP-seq on consensus sequences of Satellites **(B)** or Rhino-dependent transposons **(C)** in ovaries with indicated genetic backgrounds. Jitter plots depicting the length-normalized antisense PIWI-interacting RNA (piRNA) counts on Satellite consensus sequences derived from ovaries **(D)** or

Figure 5 continued on next page

Figure 5 continued

testes (**G**) of indicated genetic backgrounds. Box plots depicting the log2-fold change of piRNA counts (compared to w^{1118} control) per 1-kb tile for major piRNA clusters in ovaries (**E**) or testes (**F**) of the indicated genotypes. The number of tiles per piRNA cluster is indicated (n).

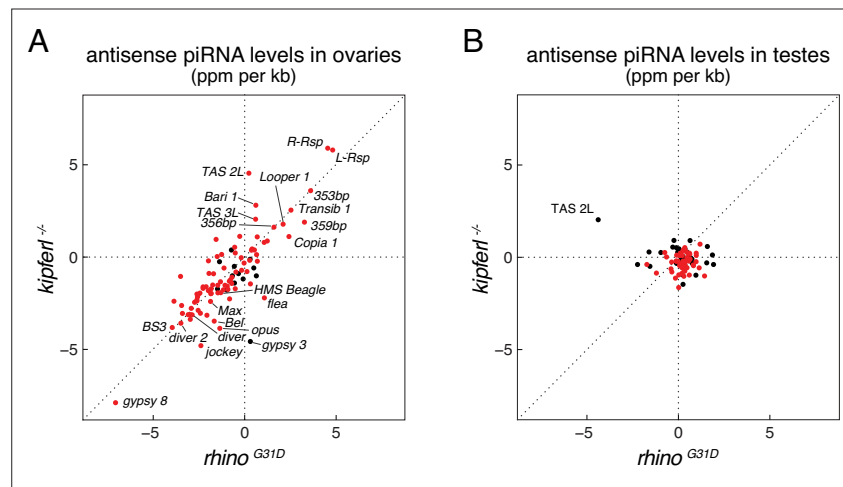


Figure 5—figure supplement 1. Antisense piRNA levels in *rhino*^{G31D} mutants resemble those in *kipferl* null mutant. Scatter plots depicting the levels of antisense PIWI-interacting RNAs (piRNAs) mapping to transposon consensus sequences in ovaries (A) and testes (B). Rhino-dependent elements are indicated in red.

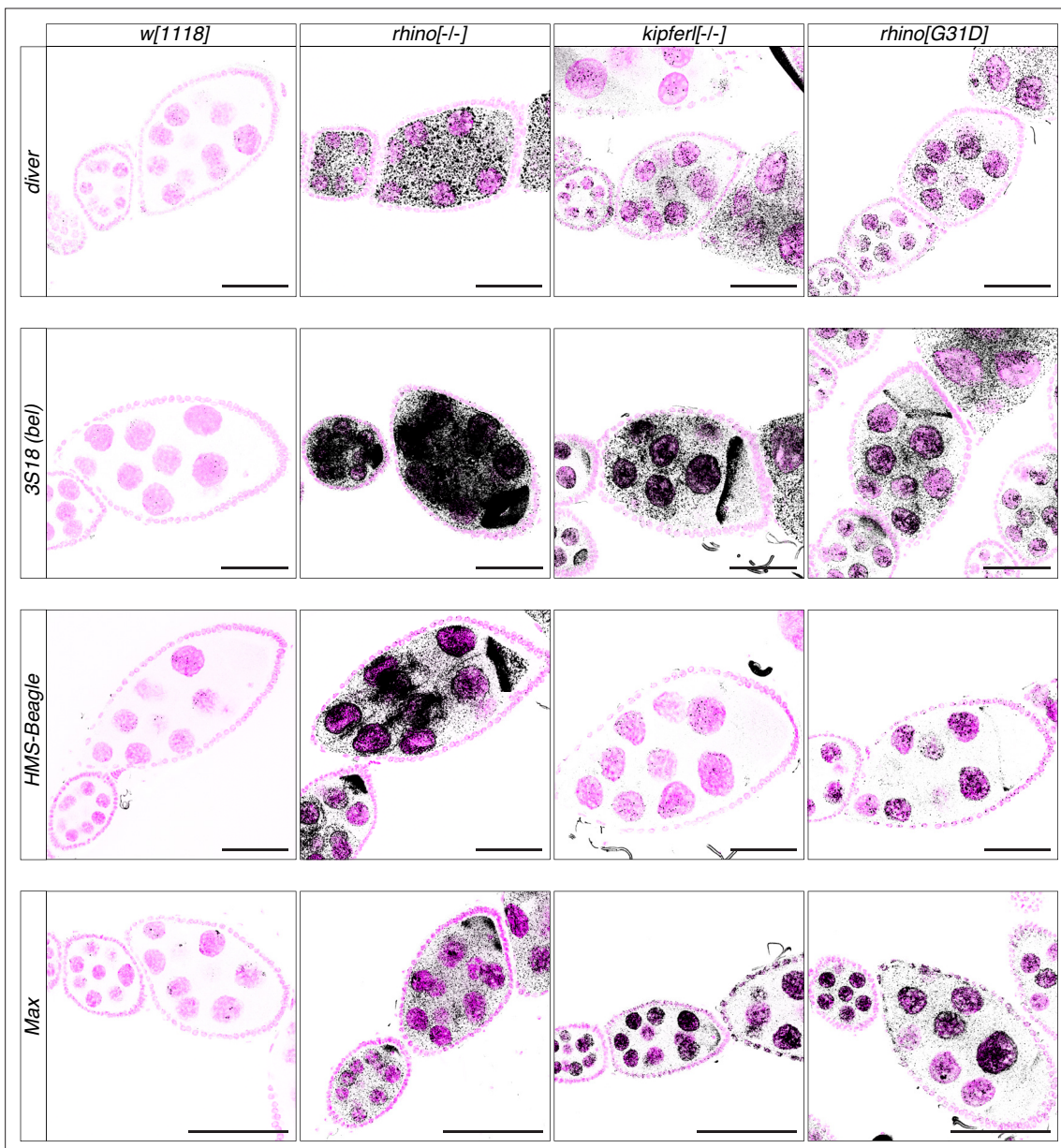


Figure 5—figure supplement 2. Transposon upregulation visualized by RNA fluorescent in situ hybridization (FISH). Confocal images showing RNA fluorescent in situ hybridization (FISH) signal (black) for transcripts of indicated transposons in *w¹¹¹⁸*, *kipferl*, or *rhino* null mutant, as well as *rhino^{G31D}* ovaries. DAPI-stained nuclei are displayed in pink (scale bars: 50 μ m).